INTERNATIONAL JOURNAL FOR NUMERICAL METHODS IN FLUIDS, VOL. 20, 75–94 (1995)

# TRANSONIC EULER COMPUTATION IN STREAMFUNCTION CO-ORDINATES

C.-F. AN AND R. M. BARRON*

*Department of Mathematics and Statistics and Fluid Dynamics Research Institute, University of Windsor, Windsor, Ontario Canada, N9B 3P4*

SUMMARY

A new approach has been developed to calculate two-dimensional steady transonic flows past aerofoils using the Euler equations in streamfunction co-ordinates. Most existing transonic computation codes require the use of a grid generator to determine a suitable distribution of grid points. Although simple in concept, the grid generation may take a considerable proportion of the CPU time and storage requirements. However, this grid generation step can be avoided by introducing the von Mises transformation, which produces a formulation in streamwise and natural body-fitting co-ordinates. In this work a set of Euler equivalent equations in streamfunction co-ordinates is formulated, consisting of three equations with three unknowns; one is a geometric variable, the streamline ordinate $y$, and the other two are physical quantities, the density $\rho$ and the vorticity $\omega$. To solve these equations, type-dependent differencing, development of a shock point operator, marching from a non-characteristic boundary and successive line overrelaxation are applied. Particular attention has been paid to the supercritical case where a careful treatment of the shock is essential. It is shown that the shock point operator is crucial to accurately capture shock waves. The computed results show excellent agreement with existing experimental data and other computations.

KEY WORDS Euler equations Streamfunction co-ordinates

## INTRODUCTION

Transonic flow is a widely encountered phenomenon in aeronautics and astronautics, occurring in flows past aerofoils, wings, through nozzle throats, cascade blades or around blunt bodies, etc. Transonic flow is more difficult to solve compared with pure subsonic or supersonic flows, because the flow fields have mixed zones and shock waves. Owing to these difficulties, there was little progress in transonic computations until the early 1970s. Since then the numerical simulation of transonic flow has been an active research topic for computational fluid dynamicists working in applied mathematics and aeronautical and aerospace engineering. The earliest efforts on transonic computation used the transonic small-disturbance (TSD) equation[1–4] and subsequently methods were developed for the full potential equations.[5–9] During the last decade attention has turned to the most accurate model for inviscid transonic computation, the Euler equations. Typical approaches include the implicit finite difference scheme,[10] the implicit approximate factorization method,[11] the finite volume scheme with explicit Runge–Kutta time stepping,[12] the flux-vector-splitting method,[13] the multigrid scheme,[14] the total-variation-diminishing scheme[15] and the finite element method.[16]

As an alternative to the above approaches, several researchers have replaced the primitive variable formulation of the Euler equations with a streamfunction–vorticity formulation and have successfully computed transonic flows.[17–22]

* Author to whom correspondence should be addressed.

CCC 0271–2091/95/010075–20

*Received 28 August 1992*
*Revised 31 August 1993*

In most CFD applications grid generation is a necessary first step in order to provide a body-fitting mesh system and this process may exhaust a considerable portion of CPU time. Hence the degree to which a numerical method can reduce this portion of time is an important index of its efficiency and applicability. Conventional numerical grid generation can be completely avoided by introducing the von Mises transformation and the corresponding streamfunction co-ordinates (SFCs). The von Mises transformation is a streamline-based co-ordinate transformation which analytically produces a body-fitting co-ordinate system. The transformation allows a single set of equations to play a double role, i.e. simultaneously serving as governing equations (flow physics) and grid generation equations (flow geometry). Therefore in recent years streamfunction (or streamline) co-ordinates have been exploited for the computation of 2D and axisymmetric incompressible potential flows,[23–28] incompressible viscous flows[29–31] and compressible potential flows.[32–40] Similar ideas have been used in turbomachinery analysis and design.[41–43]

In this study a technique is developed to calculate two-dimensional steady transonic flows past aerofoils using the Euler equations in streamfunction co-ordinates. Introducing the streamfunction and the von Mises transformation, a set of Euler equivalent equations in streamfunction co-ordinates is formulated. It consists of three coupled equations with three unknowns; one is a geometrical variable, the streamline ordinate $y$, and the other two are physical quantities, the density $\rho$ and the vorticity $\omega$. To solve the "main equation' for $y$, which is a second-order partial differential equation, a type-dependent difference scheme is applied. To treat the embedded shock wave, the shock jump conditions are analysed and a shock point operator is constructed in streamfunction co-ordinates. In order to solve for the density $\rho$, researchers traditionally use the Bernoulli equation. In the transonic range, however, the classical double-density problem exists in the new streamfunction co-ordinate formulation. Even if the artificial density technique is applied, in conjunction with the use of upwind differencing in supersonic regions, the supersonic pocket and shock waves are still difficult to handle. This is perhaps because there is no obvious mechanism by which the artificial density can provide dissipation to the $y$-equation, in the sense explained by Jameson[6] or Hafez *et al.*[7] for the potential equation and by Habashi and Hafez[17] or Hafez and Lovell[18] for the streamfunction equation. To overcome this difficulty, instead of solving the algebraic Bernoulli equation, a first-order partial differential equation called the 'secondary equation' is solved to avoid the double-density problem. Once $y$ and $\rho$ are obtained, $\omega$ can be easily calculated.

In Section 2 the Euler equivalent equations are formulated in streamfunction co-ordinates. In Section 3 the related numerical methodologies are discussed. Particular attention has been paid to the shock wave treatment, including the analysis of the shock jump conditions and the construction of the shock point operator (SPO). In Section 4 sample computations are conducted and the calculated results are compared with available experimental data and other computations. In the last section brief conclusions are given and the advantages and limitations of the present approach are discussed.

## MATHEMATICAL FORMULATION

For a two-dimensional, steady, inviscid flow around an aerofoil the most accurate mathematical model is the Euler equations

$$\begin{pmatrix} \rho u \\ \rho u^2 + p \\ \rho uv \\ \rho uH \end{pmatrix}_x + \begin{pmatrix} \rho v \\ \rho uv \\ \rho v^2 + p \\ \rho vH \end{pmatrix}_y = 0, \tag{1}$$

where $H = [\gamma/(\gamma - 1)]p/\rho + (u^2 + v^2)/2$ is the total enthalpy per unit mass, $\rho$ is the density, $u$ and $v$ are the velocity components in Cartesian co-ordinates $(x, y)$, $p$ is the pressure and $\gamma$ is the ratio of specific heats. The dependent variables $\rho$, $u$, $v$ and $p$ have been normalized by the quantities at freestream condition: density $\rho_\infty$, speed $V_\infty$ and dynamic pressure head $\rho_\infty V_\infty^2$. The independent variables $x$ and $y$ have been scaled by the aerofoil chord length.

Introducing the streamfunction $\psi$ such that

$$\psi_y = \rho u, \qquad \psi_x = -\rho v, \tag{2}$$

the continuity equation in (1) is automatically satisfied. The explicit form of the streamfunction $\psi = \psi(x, y)$ can be considered in an implicit form $F(x, y; \psi) = 0$ or in an alternative explicit form as $y = y(x, \psi)$. This process is equivalent to the introduction of the von Mises transformation[44]

$$x \equiv x, \qquad y = y(x, \psi). \tag{3}$$

If the Jacobian $J = \partial(x, y)/\partial(x, \psi) = y_\psi \neq 0, \infty$, then the transformation (3) is one-to-one and the differential operators are transformed to

$$\left.\frac{\partial}{\partial x}\right|_y = \left.\frac{\partial}{\partial x}\right|_\psi - \frac{y_x}{y_\psi}\frac{\partial}{\partial \psi}, \qquad \frac{\partial}{\partial y} = \frac{1}{y_\psi}\frac{\partial}{\partial \psi}. \tag{4}$$

Therefore the Euler equations in streamfunction co- ordinates become

$$\begin{pmatrix} 1/\rho y_\psi + p y_\psi \\ y_x/\rho y_\psi \\ H \end{pmatrix}_x + \begin{pmatrix} -p y_x \\ p \\ 0 \end{pmatrix}_\psi = 0, \tag{5}$$

where

$$H = \frac{\gamma}{\gamma - 1}\frac{p}{\rho} + \frac{1 + y_x^2}{2\rho^2 y_\psi^2}.$$

The co-ordinates $(x, \psi)$ are referred to as the streamfunction co-ordinates (SFCs)[34] and the Euler equations in streamfunction co-ordinates, (5), are completely equivalent to the Euler equations in Cartesian co-ordinates, (1), as long as the von Mises transformation (3) is valid in the problem under consideration. In this new formulation there are three dependent variables: streamline ordinate $y$, density $\rho$ and pressure $p$; as unknown functions of two independent variables: abscissa $x$ and streamfunction $\psi$.

The last equation in (5), $H_x = 0$, means that the total enthalpy $H$ is invariant along a streamline. However, for a flow with uniform freestream $H$ is invariant along any line and hence $H$ is a constant throughout the flow field. This is the so-called homoenergetic condition which is satisfied in most practical problems. The constant can be evaluated at freestream condition as

$$H = H_\infty = \tfrac{1}{2} + \frac{1}{(\gamma - 1)M_\infty^2}. \tag{6}$$

Thus equations (5) can be rewritten as

$$\left[\frac{1}{\rho y_\psi} + p y_\psi\right]_x - [p y_x]_\psi = 0, \tag{7}$$

$$\left[\frac{y_x}{\rho y_\psi}\right]_x + p_\psi = 0, \tag{8}$$

$$\frac{\gamma}{\gamma - 1}\frac{p}{\rho} = H_\infty - \frac{1 + y_x^2}{2\rho^2 y_\psi^2}. \tag{9}$$

Here the energy equation has been reduced to an algebraic equation for $p$, $\rho$ and derivatives of $y$ owing to the homoenergetic condition. The velocity components can be calculated from

$$u = \frac{1}{\rho y_\psi}, \qquad v = \frac{y_x}{\rho y_\psi} \tag{10}$$

in streamfunction co-ordinates.

Differentiating (9) with respect to $x$ and $\psi$ and substituting $p_x$ and $p_\psi$ into (7) and (8) yields

$$2y_x y_\psi^2 y_{xx} + 2y_\psi\left(\frac{1}{\gamma-1} - 2y_x^2\right)y_{x\psi} + 2y_x(1+y_x^2)y_{\psi\psi}$$
$$= y_\psi^2\left(2H_\infty\rho^2 y_\psi^2 - \frac{\gamma+1}{\gamma-1} + y_x^2\right)\frac{\rho_x}{\rho} - y_x y_\psi(2H_\infty\rho^2 y_\psi^2 + 1 + y_x^2)\frac{\rho_\psi}{\rho}, \tag{11}$$

$$\frac{2\gamma}{\gamma-1}y_\psi^2 y_{xx} - \frac{2(2\gamma-1)}{\gamma-1}y_x y_\psi y_{x\psi} + 2(1+y_x^2)y_{\psi\psi} = \frac{2\gamma}{\gamma-1}y_x y_\psi^2\frac{\rho_x}{\rho} - y_\psi(2H_\infty\rho^2 y_\psi^2 + 1 + y_x^2)\frac{\rho_\psi}{\rho}. \tag{12}$$

Then, using the definition of vorticity ($\omega = v_x - u_y$) in streamfunction co-ordinates,[36]

$$\omega = \frac{1}{y_\psi}\left(\left[\frac{y_x}{\rho}\right]_x - \left[\frac{1+y_x^2}{\rho y_\psi}\right]_\psi\right), \tag{13}$$

and eliminating $\rho_x/\rho$ and $\rho_\psi/\rho$ using (11) and (12), we get

$$(y_\psi^2 - Z_1)y_{xx} - 2y_x y_\psi y_{x\psi} + (1+y_x^2)y_{\psi\psi} = Z_2, \tag{14}$$

where

$$Z_1 = \frac{[2/(\gamma-1)]y_\psi^2}{2H_\infty\rho^2 y_\psi^2 - (1+y_x^2)}, \qquad Z_2 = \rho\omega y_\psi^3\frac{2H_\infty\rho^2 y_\psi^2 + 1 + y_x^2}{2H_\infty\rho^2 y_\psi^2 - (1+y_x^2)}$$

are the terms representing compressibility and rotational effects respectively. Equation (14), which can be solved for $y$ if $\rho$ and $\omega$ are known, is a second-order non-linear non-homogeneous partial differential equation. To classify this equation, one can show that its discriminant is

$$\Delta = 4y_\psi^2(M^2 - 1), \tag{15}$$

where $M$ is the local Mach number. Thus we observe that if the local flow is supersonic (or subsonic), then the governing equation must be hyperbolic (or elliptic) and vice versa. Therefore the mathematical classification of the governing equation in streamfunction co-ordinates is consistent with the physical nature of the local flow. This feature provides the possibility of applying the type-dependent difference scheme originally proposed by Murman and Cole[1] to numerically solve equation (14) for $y$.

It is obvious that equation (14) for $y$ is coupled with $\rho$ and $\omega$ through $Z_1$ and $Z_2$. Therefore, to solve equation (14) for $y$ iteratively, $\rho$ and $\omega$ must be updated from iteration to iteration. The density can be updated from a first-order non-linear partial differential equation obtained by eliminating the term $y_\psi^2 y_{xx} - 2y_x y_\psi y_{x\psi} + (1+y_x^2)y_{\psi\psi}$ from (13) and (14),

$$y_x y_\psi^2\rho_x - y_\psi(1+y_x^2)\rho_\psi = (Z_1 y_{xx} + Z_3)\rho, \tag{16}$$

where

$$Z_3 = \frac{2\rho\omega y_\psi^3(1+y_x^2)}{2H_\infty\rho^2 y_\psi^2 - (1+y_x^2)}$$

is the rotational term. The slope of the characteristic curve for this equation is

$$\frac{d\psi}{dx} = -\frac{1+y_x^2}{y_x\, y_\psi}. \tag{17}$$

At infinity $y_x \to 0$, $y_\psi \to 1$ and hence $d\psi/dx \to \infty$. Therefore the characteristic curve of (16) at infinity is a vertical line in the $(x, \psi)$-plane.

After $y$ is solved from (14) and $\rho$ is updated from (16), the vorticity $\omega$ can be updated from its definition (13). These equations constitute a complete set of 'Euler equivalent equations' in streamfunction co-ordinates. For convenience equation (14) is referred to as the 'main equation' for the corresponding 'main variable' $y$ and the other equations are referred to as the "secondary equations' for the related "secondary variables' $\rho$ and $\omega$. Having obtained $y$, $\rho$ and $\omega$, the local Mach number can be obtained from

$$M^2 = \frac{[2/(\gamma-1)](1+y_x^2)}{2H_\infty\rho^2 y_\psi^2 - (1+y_x^2)} \tag{18}$$

and the pressure coefficient from

$$C_p = 2\left(p - \frac{1}{\gamma M_\infty^2}\right), \tag{19}$$

where

$$p = \frac{\gamma-1}{\gamma}\left(H_\infty\rho - \frac{1+y_x^2}{2\rho y_\psi^2}\right).$$

## NUMERICAL METHODOLOGIES

Suppose an aerofoil is placed in a two-dimensional air flow with freestream Mach number $M_\infty$ at an angle of attack $\alpha$. From the previous section the governing Euler equivalent equations in streamfunction co-ordinates are composed of (14), (16) and (13)

$$(y_\psi^2 - Z_1)y_{xx} - 2y_x y_\psi y_{x\psi} + (1+y_x^2)y_{\psi\psi} = Z_2, \tag{20}$$

$$y_x y_\psi^2 \rho_x - y_\psi(1+y_x^2)\rho_\psi = (Z_1\, y_{xx} + Z_3)\rho, \tag{21}$$

$$\omega = \frac{1}{y_\psi}\left(\left[\frac{y_x}{\rho}\right]_x - \left[\frac{1+y_x^2}{\rho y_\psi}\right]_\psi\right). \tag{22}$$

On the aerofoil the boundary condition for $y$ is Dirichlet,

$$y = f_\pm(x), \tag{23}$$

where $f_+(x)$ and $f_-(x)$ represent the shape functions of the upper and lower surfaces of the aerofoil respectively. In the far field the streamfunction can be expressed by the sum of a uniform flow, a doublet and a vortex.[20] In most cases the doublet term is sufficiently small and can be ignored.

Therefore the boundary condition at infinity is given in an explicit form for $\psi$,

$$\psi(x\ y) = y\cos\alpha - x\sin\alpha + \frac{\Gamma}{2\pi}\ln[x^2 + (1 - M_\infty^2)y^2],$$

in the physical domain or in an implicit form for $y$,

$$y(x,\ \psi) = \frac{\psi}{\cos\alpha} + x\tan\alpha - \frac{\Gamma}{2\pi\cos\alpha}\ln\{x^2 + (1 - M_\infty^2)[y(x,\ \psi)]^2\}, \tag{24}$$

in the computational domain. This algebraic equation for $y = y(x, \psi)$ is non-linear and an iteration algorithm (e.g. Newton's iteration) must be applied. In addition, the Kutta condition must be satisfied, i.e. the pressures

$$p_{\mathrm{TE}} = \frac{\gamma - 1}{\gamma}\left(H_\infty\rho - \frac{1 + y_x^2}{2\rho y_\psi^2}\right)_{\mathrm{TE}} \tag{25}$$

calculated from the upper and lower surfaces at the trailing edge must be equal to each other. Sketches of the physical and computational domains and the boundary conditions are shown in Figures 1(a) and 1(b) respectively.

*Type-dependent scheme for the main equation*

Since the main equation (20) is well classified as hyperbolic- or elliptic-type depending on whether the local flow is supersonic or subsonic, it is possible to apply the type-dependent scheme to solve for $y$. Equation (20) can be rewritten as

$$A_1 y_{xx} + A_2 y_{x\psi} + A_3 y_{\psi\psi} = A_4, \tag{26}$$

where

$$A_1 = y_\psi^2 - Z_1, \qquad A_2 = -2y_x y_\psi, \qquad A_3 = 1 + y_x^2, \qquad A_4 = Z_2.$$

The type-dependent scheme reads

$$\{A_1[v\Delta_x + (1 - v)\nabla_x]\nabla_x + A_2[v\delta_x + (1 - v)\nabla_x]\delta_\psi + A_3\delta_{\psi\psi}\}y_{i,j} = A_4, \tag{27}$$

where $\Delta$, $\nabla$ and $\delta$ are forward, backward and central difference quotient operators respectively, and the switch parameter

$$v = \begin{cases} 1 & \text{for subsonic points,} \\ 0 & \text{for supersonic points.} \end{cases} \tag{28}$$

In this formulation, upwinding in the $x$-direction at supersonic points has the effect of a rotated difference scheme, since the backward differencing is actually in the direction of the streamline.

Expanding the type-dependent scheme (27) and rearranging the terms to express it in a tridiagonal coefficient matrix form, one gets

$$Ay_{i,j-1} + By_{i,j} + Cy_{i,j+1} = \mathrm{RHS}, \tag{29}$$

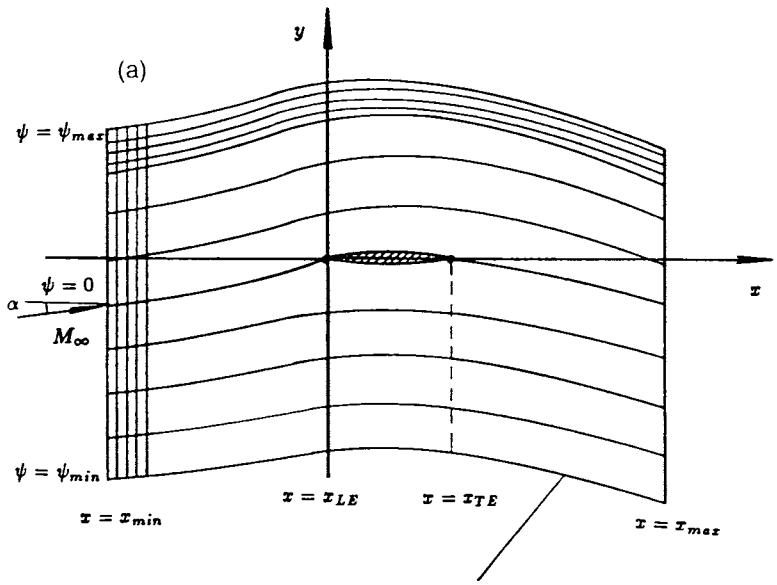


$$\psi(x,y) = y\cos\alpha - x\sin\alpha + \frac{\Gamma}{2\pi} ln\{x^2 + (1 - M_\infty^2)y^2\}$$

Figure 1(a). Physical plane

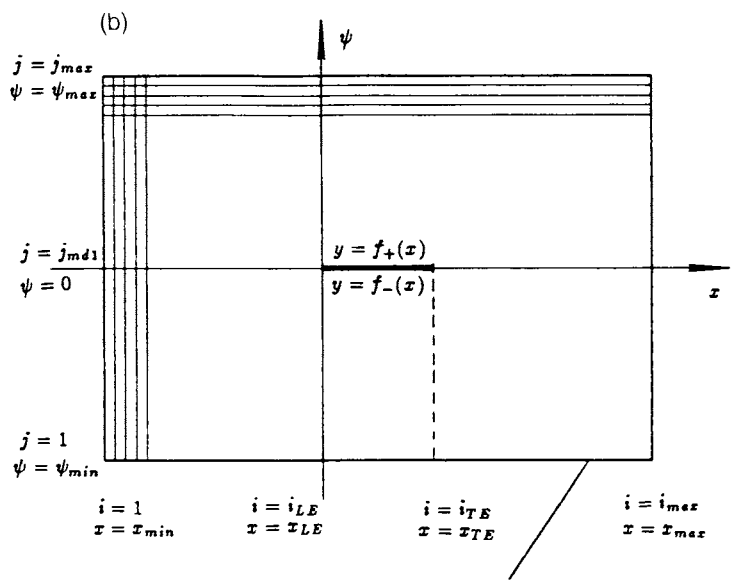


$$y(x,\psi) = \frac{\psi}{\cos\alpha} + x\tan\alpha - \frac{\Gamma}{2\pi\cos\alpha} ln\{x^2 + (1 - M_\infty^2)[y(x,\psi)]^2\}$$

Figure 1(b). Computational plane

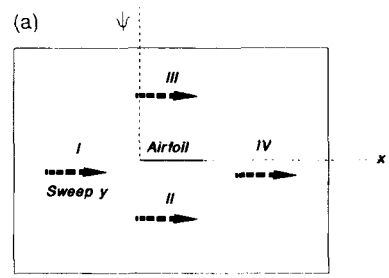


Figure 2(a). $y$-Equation sweeping

where

$$A = \beta^2 A_3 - (1-\nu)\beta A_2/2, \qquad B = -2\beta^2 A_3 + (1-3\nu)A_1, \qquad C = \beta^2 A_3 + (1-\nu)\beta A_2/2,$$

$$\begin{aligned}\text{RHS} = &-\nu A_1(y_{i+1,j} + y_{i-1,j}) + (1-\nu)A_1(2y_{i-1,j} - y_{i-2,j})\\ &-\nu\beta A_2(y_{i+1,j+1} - y_{i+1,j-1} - y_{i-1,j+1} + y_{i-1,j-1})/4\\ &+(1-\nu)\beta A_2(y_{i-1,j+1} - y_{i-1,j-1})/2 + \Delta x^2 A_4\end{aligned}$$

for $i = 2, 3, \ldots, I_{\max-1}$, $j = 2, 3, \ldots, J_{\max-1}$ and $\beta = \Delta x/\Delta\psi$.

The computational domain is divided into four subdomains as shown in Figure 2(a) and each subdomain is swept sequentially by SLOR from left to right. The whole process should be iterated up to convergence owing to the non-linearity of the equation.

*Marching the secondary equation*

Since the secondary equation (21) has vertical characteristics in the far field, it can be solved by marching line-by-line from the horizontal far-field boundary, which is a non-characteristic curve at which $\rho$=1. In our case equation (21) can be marched to the aerofoil from lower and upper boundaries for lower and upper half-planes respectively (Figure 2(b)). Equation (21) can be rewritten as

$$B_1\rho_x + B_2\rho_\psi + B_3\rho = 0, \tag{30}$$

where

$$B_1 = y_x y_\psi^2, \qquad B_2 = -y_\psi(1 + y_x^2), \qquad B_3 = -(Z_1 y_{xx} + Z_3).$$

Applying the Crank–Nicholson scheme to (30) at point $(i, j-\frac{1}{2})$ for the lower half-plane, evaluating the density $\rho$ at level $j-\frac{1}{2}$ by the average at levels $j$ and $j-1$ and rearranging the equations in a

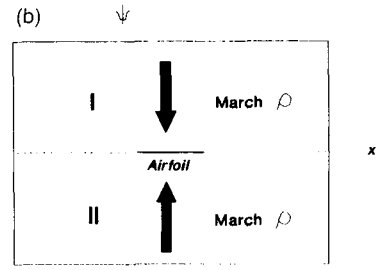


Figure 2(b). Density equation marching

tridiagonal form, one gets

$$\tilde{A}\rho_{i-1,j} + \tilde{B}\rho_{i,j} + \tilde{C}\rho_{i+1,j} = \widetilde{\mathrm{RHS}}, \tag{31}$$

where

$$\begin{aligned} &\tilde{A} = -B_1, \qquad \tilde{B} = 4\beta B_2 + 2\Delta x B_3, \qquad \tilde{C} = B_1, \\ &\widetilde{\mathrm{RHS}} = B_1\rho_{i-1,j-1} + (4\beta B_2 - 2\Delta x B_3)\rho_{i,j-1} - B_1\rho_{i+1,j-1} \end{aligned} \tag{32}$$

for $i = 2, 3, \ldots, I_{\max-1}$ and $j = 2, 3, \ldots, J_{\mathrm{mdl}}$. Here $J_{\mathrm{mdl}}$ represents the streamline coinciding with the aerofoil surface. It should be noted that $B_1$, $B_2$ and $B_3$ are taken as the averages of the corresponding quantities at $j$ and $j-1$. A similar expression holds for the upper half-plane. Along the zero streamline upstream and downstream of the aerofoil the density $\rho$ should be evaluated by averaging the values from upper and lower half-planes after each iteration. At convergence these values will be the same.

The system of difference equations (31) has a tridiagonal coefficient matrix and can be solved line-by-line horizontally using SLOR from the far- field boundaries to the aerofoil. An iterative procedure is used, because (30) is non-linear. It should also be pointed out that the second derivative $y_{xx}$ in $B_3$ should be type-dependently differenced to keep consistency with the $y$-equation. After $\rho$ is solved, the vorticity can be updated from (22) and the local Mach number can be calculated from (18). Finally, the Kutta condition requires that the pressures at the trailing edge calculated from the upper surface, $p_{\mathrm{TE}}^{+}$ and from the lower surface, $p_{\mathrm{TE}}^{-}$ must be equal to each other. That is,

$$(\Delta p)_{\mathrm{TE}} = p_{\mathrm{TE}}^{+} - p_{\mathrm{TE}}^{-} = 0, \tag{33}$$

where the pressures $p_{\mathrm{TE}}^{\pm}$ are given by (25). If (23) is not satisfied, the circulation $\Gamma$ around the aerofoil can be corrected from the expression

$$\Gamma^{(n+1)} = \Gamma^{(n)} + \beta_0(\Delta p)_{\mathrm{TE}}, \tag{34}$$

where the superscripts $(n)$ and $(n+1)$ indicate the iteration levels and the relaxation parameter $\beta_0$ can be determined from numerical tests. The numerical solution process can be described as below.

First, the tridiagonal system of algebraic equations (29) is solved for $y$ along a vertical line. Each vertical line is then successively relaxed from left to right in each subdomain and the subdomains are swept in the order I, II, III and IV. Each time after $y$ is relaxed, the error between the current and previous iterations is checked for all grid points. If the error is less than the prescribed tolerance, the iterations are considered to be converged, otherwise the iterations are repeated until convergence. After $y$ is converged, $\rho$ can be solved from equation (31). The tridiagonal system of algebraic equations (31) is solved along a horizontal line and each horizontal line is marched upwards or downwards to the aerofoil. After $\rho$ is converged, the Mach number $M$ and vorticity $\omega$ are calculated and the Kutta condition (33) is checked. If it is not satisfied, $\Gamma$ is updated using (34) and the procedure is repeated again up to convergence. The Mach number is used to distinguish the grid point type: subsonic, supersonic or shock wave. The computational flowchart is shown in Figure 3.

*Shock jump condition*

As might be expected, numerical tests indicated that the type-dependent scheme is effective only for subcritical flows and for supercritical flows with weak shock waves. For a supercritical flow with moderate or strong shock waves the computation either fails to converge or is forced to stop owing to inaccurate intermediate values of the unknowns $y$ and $\rho$ during the process of iteration. Occasionally the computation converges but gives inaccurate pressure distributions and incorrect shock wave

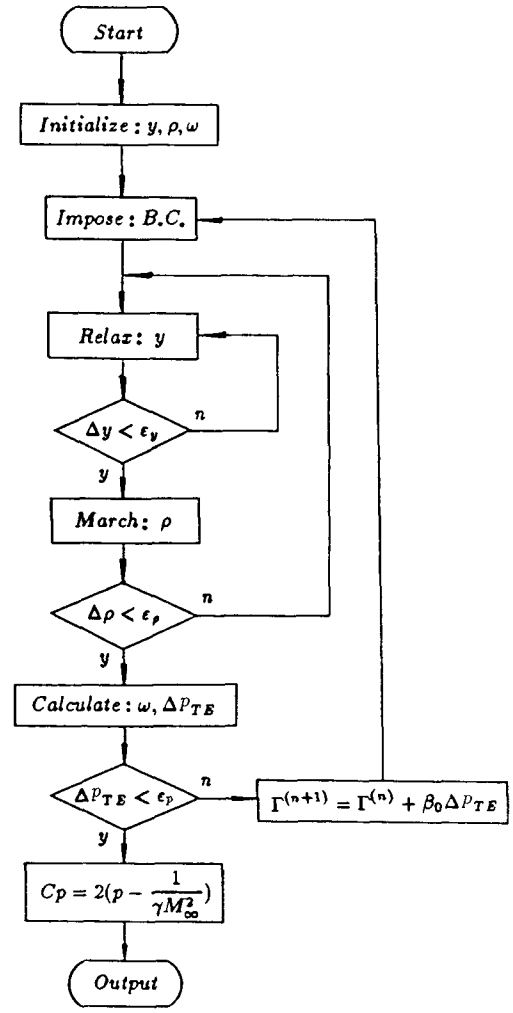


Figure 3. Computational flow chart

positions. This means that the shock waves are not being properly handled. Therefore a special treatment of shock waves is necessary. In the early work of Murman and Cole[1] the shock jump conditions are automatically incorporated in their scheme for the TSD equation. The sonic line and weak shock waves develop naturally during the course of iteration. No special shock wave treatment has been made in their computation. To improve this approach, Murman[2] proposed the concept of shock point operator (SPO) for the TSD equation and was able to achieve an improved solution. Although Murman's SPO cannot be applied here directly, the basic idea and analysis of the shock wave structure provide a useful hint for extension to more accurate models such as full potential or Euler equations.

Suppose an oblique shock wave makes an angle $\beta$ with the $x$-axis. Let $V$ and $\alpha$ be the velocity and its angle with the $x$-axis, $u$ and $v$ be the $x$- and $y$-velocity components and $V_n$ and $V_t$ be the normal and tangential velocity components to the shock. Superscripts '$\mp$' represent upstream and downstream of the shock (Figure 4(a)). The tangential shock relation $V_t^+ = V_t^-$ gives

$$V^+ \cos(\beta - \alpha^+) = V^- \cos(\beta - \alpha^-).$$

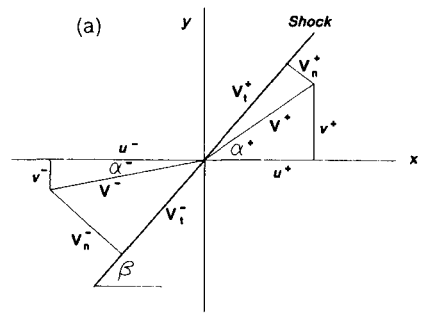


Figure 4(a). Shock jump condition

Expanding this equation and using the relations $u^{\pm} = V^{\pm} \cos \alpha^{\pm}$ and $v^{\pm} = V^{\pm} \sin \alpha^{\pm}$ yields

$$\frac{v^+ - v^-}{u^+ - u^-} = -K, \tag{35}$$

where $K = 1/\tan \beta$ is the reciprocal of the shock wave slope. Similarly the normal shock relation $\rho^+ V_n^+ = \rho^- V_n^-$ gives

$$\frac{\rho^+ u^+ - \rho^- u^-}{\rho^+ v^+ - \rho^- v^-} = K. \tag{36}$$

Equations (35) and (36) can be expressed in a compact form

$$[v] + K[u] = 0, \qquad [\rho u] - K[\rho v] = 0, \tag{37}$$

where [...] represents the jump of the corresponding quantities across the shock wave. Recalling that $\rho u y_\psi = 1$ and $v = y_x u$, the oblique shock jump conditions in streamfunction co-ordinates are

$$\left[\frac{y_x}{\rho y_\psi}\right] + K\left[\frac{1}{\rho y_\psi}\right] = 0, \qquad \left[\frac{1}{y_\psi}\right] - K\left[\frac{y_x}{y_\psi}\right] = 0. \tag{38}$$

For a shock wave which is perpendicular to the $x$-axis, $\beta = \pi/2$, $K = 0$ and the shock jump conditions reduce to

$$\left[\frac{y_x}{\rho}\right] = 0, \qquad [y_\psi] = 0. \tag{39}$$

These are the normal shock jump conditions in streamfunction co-ordinates.

*Shock point operator*

For moderate transonic Mach number the shock wave is approximately normal and can therefore be assumed to be an infinitely thin discontinuity surface located at point $(i - \frac{1}{2}, j)$ and perpendicular to the $x$-axis (Figure 4(b)). The shock jump conditions (39) can be written as

$$y_x^+ = \mu y_x^-, \qquad y_\psi^+ = y_\psi^-, \tag{40}$$

where

$$\mu = \frac{\rho^+}{\rho^-} = \frac{[(\gamma + 1)/2](M^2)^-}{1 + [(\gamma - 1)/2](M^2)^-}$$

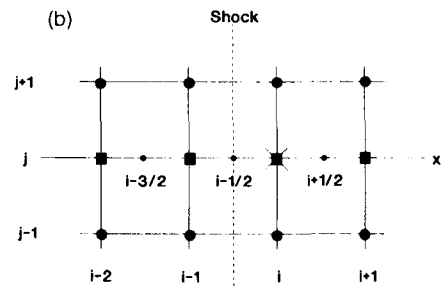

Figure 4(b). Shock point operator

is the density jump factor and can be evaluated from the Rankine–Hugoniot relation. The squared Mach number at point $(i-\frac{1}{2},\ j)^-$ can be evaluated by extrapolation from the two upstream grid points $(i-1,\ j)$ and $(i-2,\ j)$ as

$$(M^2)^-_{i-1/2,j} = \tfrac{3}{2}M^2_{i-1,j} - \tfrac{1}{2}M^2_{i-2,j}.$$

Thus the shock jump conditions (40) can be rewritten as

$$(y_x)^+_{i-1/2,j} = \mu_j (y_x)^-_{i-1/2,j}, \qquad (y_\psi)^+_{i-1/2,j} = (y_\psi)^-_{i-1/2,j}, \tag{41}$$

where

$$\mu_j = \frac{[(\gamma+1)/4](3M^2_{i-1,j} - M^2_{i-2,j})}{1 + [(\gamma-1)/4](3M^2_{i-1,j} - M^2_{i-2,j})}$$

is the density jump factor on the $j$th streamline. Finally we construct the difference approximation to $y_{xx}$ at a shock point $i = i_s$, i.e. the grid point just behind the shock, so that for $i_s$ we have

$$\begin{aligned}
(y_{xx})_{i,j} &= \frac{1}{\Delta x}[(y_x)_{i+1/2,j} - (y_x)^+_{i-1/2,j}] \\
&= \frac{1}{\Delta x}[(y_x)_{i+1/2,j} - \mu_j (y_x)^-_{i-1/2,j}] \\
&= \frac{1}{\Delta x}\left(\frac{1}{\Delta x}(y_{i+1,j} - y_{i,j}) - \frac{\mu_j}{\Delta x}(y_{i-1,j} - y_{i-2,j})\right) \\
&= \frac{1}{\Delta x^2}(y_{i+1,j} - y_{i,j} - \mu_j y_{i-1,j} + \mu_j y_{i-2,j}).
\end{aligned} \tag{42}$$

Similarly the cross-derivative can be approximated by

$$\begin{aligned}
(y_{x\psi})_{i,j} &= \frac{1}{\Delta x}[(y_\psi)_{i+1/2,j} - (y_\psi)^+_{i-1/2,j}] \\
&= \frac{1}{\Delta x}[(y_\psi)_{i+1/2j} - (y_\psi)^-_{i-1/2,j}] \\
&= \frac{1}{4\Delta x \Delta \psi}(y_{i+1,j+1} - y_{i+1,j-1} + y_{i,j+1} - y_{i,j-1} - 3y_{i-1,j+1} \\
&\qquad + 3y_{i-1,j-1} + y_{i-2,j+1} - y_{i-2,j-1}).
\end{aligned} \tag{43}$$

Equations (42) and (43) define the shock point operator in streamfunction co-ordinates. Numerical tests for both full potential[40] and the present Euler calculations show that the first derivatives $y_x$, $\rho_x$,

Table I

| $M^2_{i-1,j}$ | $M^2_{i,j}$ | Local flow type at $(i,j)$ |
|---|---|---|
| <1 | <1 | Subsonic point |
| <1 | >1 | Sonic point |
| >1 | >1 | Supersonic point |
| >1 | <1 | Shock point |

etc. do not need special treatment across shock waves, although they do have jumps across the shock waves.

Owing to the special treatment of the grid point at a shock wave, the type-dependent difference scheme (29) and the Crank–Nicolson scheme (31) must be revised. The system of difference equations for $y$ is of the same form as (29), but the coefficients $A$, $B$, $C$ and the RHS term have to be modified to

$$A = \beta^2 A_3 - \begin{cases} (1-\nu)\beta A_2/2 & \text{if } i \neq i_s, \\ \beta A_2/4 & \text{if } i = i_s. \end{cases}$$

$$B = -2\beta^2 A_3 + \begin{cases} (1-3\nu)A_1 & \text{if } i \neq i_s, \\ -A_1 & \text{if } i = i_s. \end{cases}$$

$$C = \beta^2 A_3 + \begin{cases} (1-\nu)\beta A_2/2 & \text{if } i \neq i_s, \\ \beta A_2/4 & \text{if } i = i_s. \end{cases}$$

$$\text{RHS} = \begin{cases} -\nu A_1(y_{i+1,j} + y_{i-1,j}) + (1-\nu)A_1(2y_{i-1,j} - y_{i-2,j}) \\ -\nu\beta A_2(y_{i+1,j+1} - y_{i+1,j-1} - y_{i-1,j+1} + y_{i-1,j-1})/4 \\ \quad +(1-\nu)\beta A_2(y_{i-1,j+1} - y_{i-1,j-1})/2 + \Delta x^2 A_4 & \text{if } i \neq i_s, \\ -A_1(y_{i+1,j} - \mu_j y_{i-1,j} + \mu_j y_{i-2,j}) \\ -\beta A_2(y_{i+1,j+1} - y_{i+1,j-1} - 3y_{i-1,j+1} \\ \quad +3y_{i-1,j-1} + y_{i-2,j+1} - y_{i-2,j-1})/4 + \Delta x^2 A_4 & \text{if } i = i_s, \end{cases} \tag{44}$$

where $\beta = \Delta x/\Delta\psi$, $i = 2, 3, \ldots, I_{\max-1}$ and $j = 2, 3, \ldots, J_{\max-1}$.

Similar changes occur in the equation for $\rho$, i.e. (31). In particular, the second derivative $y_{xx}$ in the expression for $B_3$ should be approximated by the type-dependent difference with shock point operator.

In order to determine the type of local flow at grid point $(i,j)$, the Mach number at two adjacent grid points is checked, i.e. the current point $(i,j)$ and the immediately upstream point $(i-1,j)$. The criteria are given in Table I.

In computational practice the sonic points need not be distinguished, because there is no jump across the sonic line. However, the shock points must be identified carefully and this is a key step in supercritical transonic flow computation.

## SAMPLE COMPUTATIONS

The Euler equivalent equations in streamfunction co-ordinates have been used to calculate transonic flows past aerofoils at subcritical and supercritical Mach numbers. The computations are executed for the set of equations (29) for $y$ and (31) for $\rho$. The vorticity $\omega$ is calculated from (22) using central differences for all $x$- and $\psi$-derivatives. The iteration involves three levels of loops. The internal loop is for the $y$-iteration, the intermediate loop is for $\rho$ and the external iteration loop is for $\omega$ and $\Gamma$. For

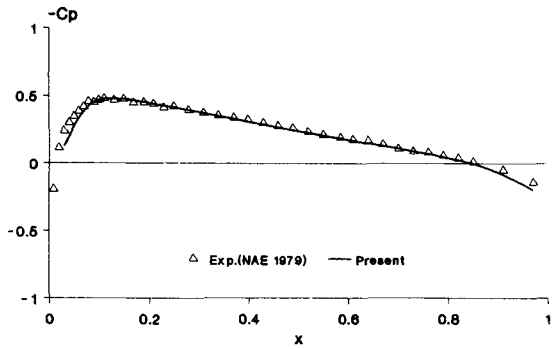


Figure 5. $C_p$ comparison: NACA 0012, $\alpha = 0°$, $M_\infty = 0{\cdot}490$

subcritical and shock-free or weak shock supercritical flows, accurate solutions are obtained on a $65 \times 65$ uniform mesh in the $(x, \psi)$-domain, which is truncated as $-2 \leq x \leq 3$, $-2{\cdot}5 \leq \psi \leq 2{\cdot}5$ with the aerofoil located between 0 and 1. For flows with moderate or strong shock waves, clustering transformations[45] are required to place a sufficient number of grid points on the aerofoil to accurately predict the locations and strengths of the shocks.

Figures 5–10 show comparisons between the calculated results and experimental data or other computations. The experimental data are extracted from work at ONERA (France),[46] NAE (Canada)[47] and NASA (U.S.A).[48] Figure 5 is the comparison of the $C_p$-distribution for NACA 0012 for purely subsonic flow at Mach number $M_\infty = 0{\cdot}490$ at zero angle of attack. Figure 6 is for NACA 0012 at $M_\infty = 0{\cdot}503$ and $\alpha = 6{\cdot}05°$. Figure 7 gives the $C_p$-distribution for NACA 0012 at slightly supercritical Mach number $M_\infty = 0{\cdot}756$ and $\alpha = 0°$. These shock-free calculations, performed on a uniform grid, show excellent agreement between computed and experimental results. Figure 8 gives the results of a supercritical calculation on a clustered grid. This example shows that the computational method described here can be used to accurately capture shock waves. Figure 9 illustrates the $C_p$-distribution on a 6% biconvex aerofoil at $M_\infty = 0{\cdot}909$ and $\alpha = 0°$ and shows excellent agreement with experiments. Excellent agreement is also seen in Figure 10, where the present calculations carried out on a clustered grid are compared with earlier test case computations[49] for $M_\infty = 0{\cdot}8$ and $\alpha = 1{\cdot}25°$. Figures 11 and 12 show the Mach number and entropy contours respectively for the same test case of NACA 0012 at $M_\infty = 0{\cdot}8$ and $\alpha = 1{\cdot}25°$.

Figure 13 demonstrates the evolution of iterations and convergence process for a typical supercritical calculation on a clustered grid: NACA 0012, $M_\infty = 0{\cdot}803$ and $\alpha = 0°$. The $C_p$-distributions

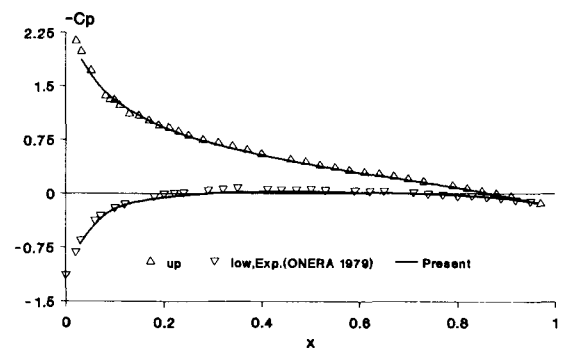


Figure 6. $C_p$ comparison: NACA 0012, $\alpha = 6{\cdot}05°$, $M_\infty = 0{\cdot}503$

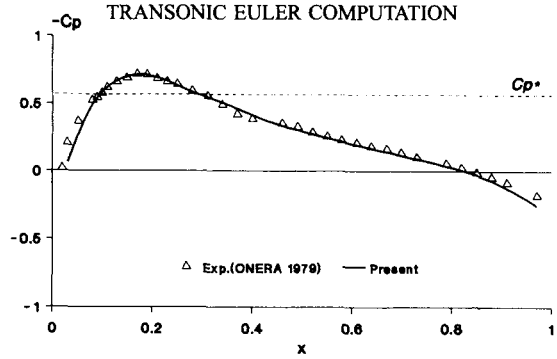


Figure 7. $C_p$ comparison: NACA 0012, $\alpha = 0°$, $M_\infty = 0{\cdot}756$

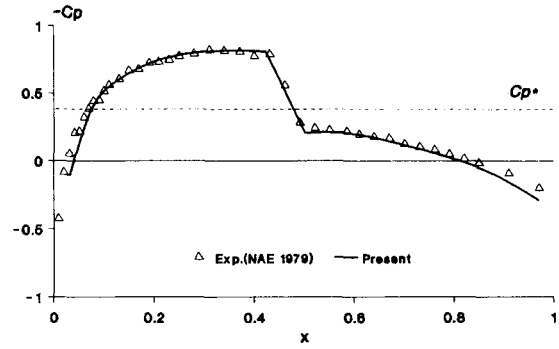


Figure 8. $C_p$ comparison: NACA 0012, $\alpha = 0°$, $M_\infty = 0{\cdot}814$

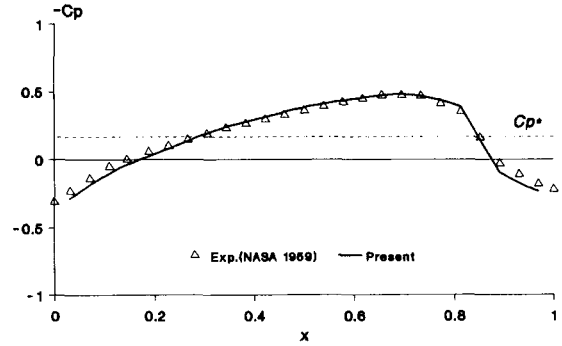


Figure 9. $C_p$ comparison: biconvex (6%) aerofoil, $\alpha = 0°$, $M_\infty = 0{\cdot}909$

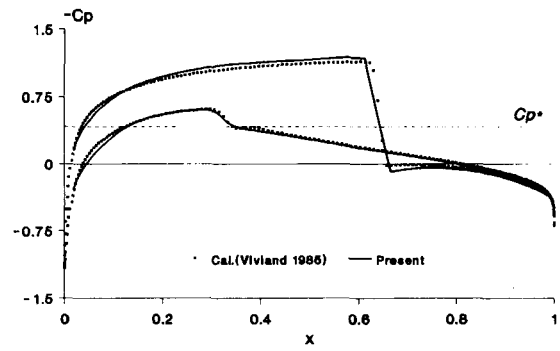


Figure 10. $C_p$ comparison: NACA 0012, $\alpha = 1{\cdot}25°$, $M_\infty = 0{\cdot}800$

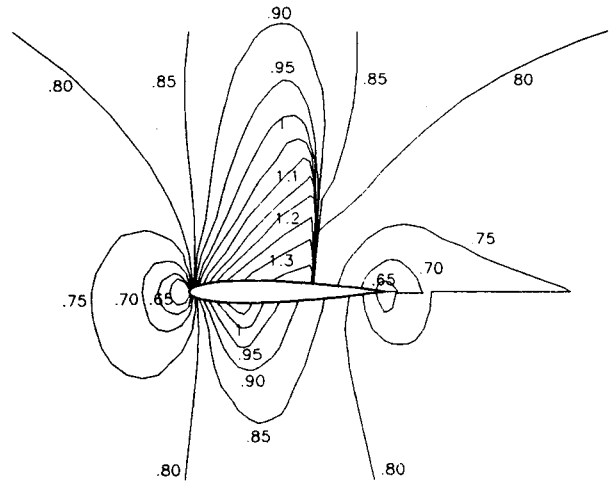


Figure 11. Mach contour: NACA 0012, $\alpha = 1{\cdot}25°$, $M_\infty = 0{\cdot}8$

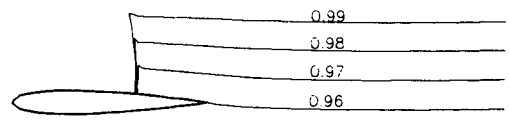


Figure 12. Total pressure contour: NACA 0012, $\alpha = 1{\cdot}25°$, $M_\infty = 0{\cdot}8$

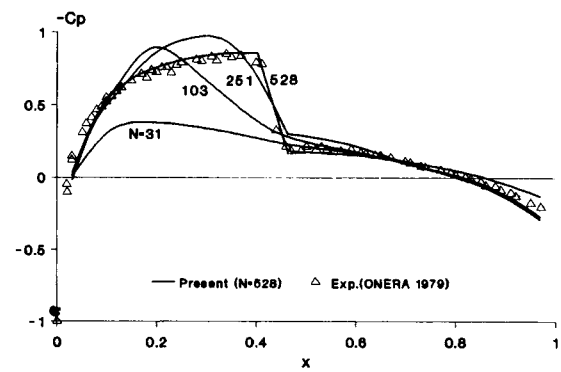


Figure 13. Evolution of iterations: NACA 0012, $\alpha = 0°$, $M_\infty = 0{\cdot}803$

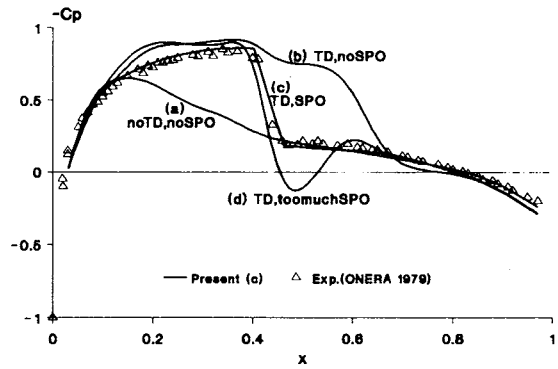


Figure 14. Effect of TD and SPO: NACA 0012, $\alpha = 0°$, $M_\infty = 0{\cdot}803$

on the aerofoil are plotted after the following numbers of iterations: 31, 103, 251 and 528. These plots show that before 251 iterations the calculated flow field has no shock wave. After 251 iterations a shock wave is formed and pushed backwards, with the accuracy improving as the iteration proceeds. The solution converges after 528 iterations and gives excellent results.

Figure 14 shows the effect of type-dependent (TD) differencing and shock point operator (SPO) in a typical supercritical calculation: NACA 0012, $M_\infty = 0{\cdot}803$ and $\alpha = 0°$. Curve (a) gives the result of central differencing with neither TD nor SPO. The $C_p$-distribution is totally unacceptable, completely missing the supercritical region and shock wave. Curve (b) shows the result of TD differencing only, without SPO. The $C_p$-distribution is inaccurate and the shock wave location is too far downstream. Curve (c) shows the result of TD differencing plus appropriate SPO, i.e. SPO is used in terms $y_{xx}$ and $y_{x\psi}$ only. The calculation gives an accurate $C_p$-distribution and shock wave location. Curve (d) shows the result of TD differencing plus too much SPO, i.e. SPO is used not only in $y_{xx}$ and $y_{x\psi}$ but also in terms $y_x$ and $\rho_x$. The $C_p$-distribution is unacceptable again and a severe oscillation occurs in the shock wave region. Comparing these curves, one can conclude that the TD differencing plus the appropriate SPO is an effective scheme to calculate transonic flows and the SPO is a crucial tool to accurately capture the embedded shock waves.

## CONCLUSIONS

The Euler equivalent equations in streamfunction co-ordinates consist of a main equation for the corresponding main (geometric) variable, the streamline ordinate $y$, and a secondary equation for the secondary (physical) variable, the density $\rho$, and an equation for the vorticity $\omega$. These three equations are coupled together and must be solved simultaneously or iteratively.

The main equation for $y$ is a second-order non-linear partial differential equation with Dirichlet boundary conditions. It is solved using type-dependent differencing plus a shock point operator. The shock point operator is a crucial numerical tool to accurately capture the embedded shock waves.

The secondary equation for $\rho$ is a first-order partial differential equation and is solved by marching vertically from far-field boundaries to the aerofoil. The Crank–Nicolson scheme is effective in solving this equation.

The approach based on the Euler equivalent equations in streamfunction co- ordinates is able to simulate transonic flows past two-dimensional aerofoils. The embedded shock waves in supercritical

flows can be accurately captured in the process of iteration. The calculated results compare favourably with existing experimental data and other computations.

## APPENDIX: NOMENCLATURE

| | |
|---|---|
| $C_p$ | pressure coefficient |
| $H$ | total enthalpy |
| $J$ | Jacobian of a transformation |
| $K$ | 1/tan $\beta$ |
| $M$ | local Mach number |
| $p$ | pressure |
| $u$, $v$ | velocity components in directions $x$ and $y$ respectively |
| $V$ | speed |
| $(x, y)$ | Cartesian co-ordinates |
| $(x, \psi)$ | streamfunction co-ordinates |

*Greek letters*

| | |
|---|---|
| $\alpha$ | angle of attack or velocity angle with $x$- axis |
| $\beta$ | $\Delta x/\Delta\psi$ or shock wave angle with $x$-axis |
| $\beta_0$ | relaxation parameter for $\Gamma$ |
| $\gamma$ | ratio of specific heats |
| $\Gamma$ | circulation |
| $\mu$ | density jump factor |
| $\nu$ | switch parameter |
| $\rho$ | density |
| $\psi$ | streamfunction |
| $\omega$ | vorticity |

*Subscripts*

| | |
|---|---|
| $i, j$ | grid points |
| LE, TE | leading and trailing edges respectively |
| $x, y, \psi$ | partial derivatives |
| $\infty$ | freestream value |

## REFERENCES

1. E. M. Murman and J. D. Cole, 'Calculation of plane steady transonic flows', *AIAA J.*, **9**, 114–121 (1971).
2. E. M. Murman, 'Analysis of embedded shock waves calculated by relaxation methods', *AIAA J.*, **12**, 626–633 (1974).
3. S. T. K. Chan, M. R. Brashears and V. Y. C. Young, 'Finite element analysis of transonic flow by the method of weighted residuals', *AIAA Paper 75-79*, 1975.
4. M. Hafez and H. K. Cheng, 'Shock-fitting applied to relaxation solutions', *AIAA J.*, **15**, 786–793 (1977).
5. A. Jameson, 'Iterative solution of transonic flows over airfoils and wings, including flows at Mach 1', *Commun. Pure Appl. Math.*, **27**, 283–309 (1974).
6. A. Jameson, "Numerical computation of transonic flows with shock waves', in K. Oswatitsch and D. Rues (eds), *Symp. Transsonicum II*, Springer, New York, 1976, pp. 384–414.
7. M. Hafez, J. South and E. M. Murman, 'Artificial compressibility methods for numerical solutions of transonic full potential equation', *AIAA J.*, **17**, 838–844 (1979).
8. T. L. Holst and W. F. Ballhaus, 'Fast conservative schemes for the full potential equation applied to transonic flows', *AIAA J.*, **17**, 145–152 (1979).
9. W. G. Habashi and M. Hafez, "Finite element solutions of transonic flow problems', *AIAA J.*, **20**, 1368–1376 (1982).
10. J. L. Steger, "Implicit finite-difference simulation of flow about arbitrary two-dimensional geometries', *AIAA J.*, **16**, 679–686 (1978).
11. T. H. Pulliam and D. S. Chaussee, 'A digital form of an implicit approximate factorization algorithm', *J. Comput. Phys.*, **39**, 347–363 (1981).

12. A. Jameson, W. Schmidt and E. Turkel, 'Numerical solution of the Euler equations by finite volume methods using Runge–Kutta time stepping schemes', *AIAA Paper 81-1259,* 1981.
13. J. L. Steger and R. F. Warming, 'Flux vector splitting of the inviscid gasdynamic equations with application of finite-difference methods', *J. Comput. Phys.,* **40**, 263–293 (1981).
14. R.-H. Ni, "A multi-grid system for solving the Euler equations', *AIAA J.,* **20**, 1565–1571 (1982).
15. A. Harten, "A high resolution scheme for the computation of weak solutions of hyperbolic conservation laws', *J. Comput. Phys.,* **49**, 357–393 (1983).
16. A. Ecer and H. U. Akay, 'A finite element formulation for steady transonic Euler equations', *AIAA J.,* **21**, 343–350 (1983).
17. W. G. Habashi and M. Hafez, Finite element stream function solutions for transonic turbomachinery flows', *AIAA Paper 82-1268,* 1982.
18. M. Hafez and D. Lovell, 'Numerical solution of transonic stream function equation', *AIAA J.,* **21**, 327–335 (1983).
19. W. G. Habashi, P. L. Kotiuga and L. A. McLean, 'Finite element simulation of transonic flows by modified potential and stream function methods', *Eng. Anal.* **2**, 150–154 (1985).
20. H. L. Atkins and H. A. Hassan, 'A new stream function formulation for the steady Euler equations', *AIAA J.,* **23**, 701–706 (1985).
21. M. Hafez and J. Ahmad, 'Numerical simulation of rotational flows', in J. Zierep and H. Oertel (eds), *Symp. Transsonicum III,* Springer, New York, 1988, pp. 339–354.
22. M. Hafez, C. Yam, K. Tang and H. Dwyer, 'Calculations of rotational flows using stream function', *AIAA Paper 89-0474,* 1989.
23. R. W. Jeppson, 'Inverse formulation and finite difference solution for flow from a circular orifice', *J. Fluid Mech.,* **40**, 215–223 (1970).
24. T. Yang and C. D. Nelson, 'Griffith diffusers', *J. Fluids Eng.,* **101**, 473–477 (1979).
25. M. S. Greywall, 'Streamwise computation of 2-D incompressible potential flows', *J. Comput. Phys.,* **59**, 224–231 (1985).
26. R. M. Barron, 'Computation of incompressible potential flow using von Mises coordinates', *Math. Comput. Simul.,* **31**, 177–188 (1989).
27. R. M. Barron, S. Zhang, A. Chandna and N. Rudraiah, 'Axisymmetric potential flow calculations. Part 1: Analysis mode', *Commun. Appl. Numer. Methods,* **6**, 437–445 (1990).
28. R. M. Barron, 'A non-iterative technique for design of aerofoils in incompressible potential flow', *Commun. Appl. Numer. Methods,* **6**, 557–564 (1990).
29. J. L. Duda and J. S. Vrentas, 'Fluid mechanics of laminar liquid jets', *Chem. Eng. Sci.,* **22**, 855–869 (1967).
30. L. R. Clermont and M. E. Lande, 'A method for the simulation of plane or axisymmetric flows of incompressible fluid based on the concept of the stream function', *Eng. Comput.,* **3**, 339–347 (1986).
31. K. Takahashi, 'A numerical analysis of flow using streamline coordinates (the case of two-dimensional steady incompressible flow)', *Bull. JSME,* **25**, 1696–1702 (1982).
32. C. E. Pearson, 'Use of streamline coordinates in the numerical solution of compressible flow problems', *J. Comput. Phys.,* **42**, 257–265 (1981).
33. D. R. Owen and C. E. Pearson, 'Numerical solution of a class of steady state Euler equations by a modified streamline method', *AIAA Paper 88-0625,* 1988.
34. C.-Y. Huang and G. S. Dulikravich, 'Stream function and stream function coordinate (SFC) formulations for inviscid flow field calculations', *Comput. Methods Appl. Mech. Eng.,* **59**, 155–177 (1986).
35. G. S. Dulikravich, 'A stream-function-coordinate (SFC) cncept in aerodynamic shape design', *AGARD VKI Lecture Series,* 1990.
36. R. M. Barron and R. K. Naeem, 'Numerical solution of transonic flows on a streamfunction co-ordinate system', *Int. j. numer. methods fluids,* **9**, 1183–1193 (1989).
37. R. K. Naeem and R. M. Barron, 'Transonic computations on a natural grid', *AIAA J.,* **28**, 1836–1838 (1990).
38. R. M. Barron and R. K. Naeem, '2-D transonic calculations on a flow- based grid system', *Math. Comput. Simul.,* **33**, 65–67 (1991).
39. R. M. Barron and C.-F. An, 'Analysis and design of transonic airfoils using streamwise coordinates', in G. S. Dulikravich (ed), *Proc. 3rd Int. Conf. on Inverse Design Concepts and Optimization in Engineering Science,* Washington, DC, 1991, pp. 359–370.
40. C.-F. An and R. M. Barron, 'Numerical solution of transonic full- potential-equivalent equations in von Mises coordinates', *Int. j. numer. methods fluids,* **15**, 925–952 (1992).
41. G.-L. Liu and C. Tao, 'A universal image-plane method for inverse and hybrid problems of compressible cascade flow on arbitrary stream sheet of revolution: part I—theory', in C. Taylor *et al.* (eds), *Numerical Methods in Laminar and Turbulent Flows,* Vol. 6, Pt. II, Pineridge, Swansea, 1989, pp. 1343–1354.
42. K.-M. Chen, D.-F. Zhang, and Z.-G. Zhu, 'A universal image-plane method for direct-, inverse- and hybrid problems of compressible cascade flow on arbitrary stream sheet of revolution: part II—numerical solution', in C. Taylor *et al.* (eds), *Numerical Methods in Laminar and Turbulent Flows,* Vol. 6, Pt. II, Pineridge, Swansea, 1989, pp. 1355–1365.
43. G.-L. Liu and D.-F. Zhang, 'The moment function formulation of inverse and hybrid problems for blade-to-blade compressible viscous flow along axisymmetric stream sheet', in C. Taylor *et al.* (eds), *Numerical Methods in Laminar and Turbulent Flows,* Vol. 6, Pt. II, Pineridge, Swansea, 1989, pp. 1289–1300.
44. R. von Mises, 'Bemerkungen zur Hydrodynamik', *ZAMM,* **7**, 425 (1927).
45. D. J. Jones and R. G. Dickinson, 'A description of the NAE two-dimensional transonic small disturbance computer method', *NAE Tech. Rep. LTR-HA-39,* 1980.

46. J. J. Thibert and M. Grandjacques, 'Experimental data base for computer program assessment', *AGARD AR-138,* 1979, pp. A1-1–A1-19.
47. L. H. Ohman, 'Experimental data base for computer program assessment', *AGARD AR-138*, 1979, pp. A1-20–A1-36.
48. E. D. Knetchtel, 'Experimental investigation at transonic speeds of pressure distributions over wedge and circular-arc-airfoil sections and evaluation of perforated wall interference', *NASA TN D-15,* 1959.
49. H. Viviand, 'Numerical solutions of two-dimensional reference test cases', *AGARD AR-211,* 1985, pp. 6-1–6-68.